



Modeling of the human mandibular periosteum material properties and comparison with the calvarial periosteum

Natacha Kadlub¹ · Alexandre Debelmas² · Jeremy Dallard² · Arnaud Picard¹ · Jean Boisson²

Received: 27 February 2019 / Accepted: 27 August 2019 / Published online: 11 September 2019
© Springer-Verlag GmbH Germany, part of Springer Nature 2019

Abstract

Knowledge of mandibular periosteum mechanical properties is fundamental for understanding its role in craniofacial growth, in trauma and bone regeneration. There is a lack in the literature regarding mechanical behavior of the human periosteum, including both experimental and modeling aspects. The proposed study involves tensile tests of periosteum samples from different locations including two locations of human mandibular periosteum: lingual and vestibular, compared with samples from various locations of the calvarial periosteum. We propose to analyze the tensile response of the mandibular periosteum using a model, initially applied on the skin, and based on a structural approach involving the mechanical properties of the corrugation of the collagen. Two different approaches for the model parameters' identification are proposed: (1) identification from experimental curve fitting and (2) identification from histological study. This approach allows us to compare parameters extracted from the traction test fitting to structural parameters measured on periosteum histological slices. Concerning experimental aspects, we showed significant differences, in terms of stiffness, between calvarial and mandibular periosteum. (The mean final stiffness is $E_{c,mand} = 18$ MPa for the mandible versus $E_{c,calv} = 70.1$ for the calvaria.) About modeling, we succeed to capture the correct mechanical behavior for the periosteum, and the statistical analysis showed that certain parameters from the geometric data and traction data are significantly comparable (e.g., $p = 0.3$ for E_c). However, we also observed a discrepancy between these two approaches for the elongation at which the fibril has become straight ($p = 0.0001$).

Keywords Elastic moduli · Young's moduli · Periosteum · Collagen · Traction test

1 Introduction

The periosteum is a bilayer fibrous soft tissue surrounding bones and involved in bone growth and repair (Evans et al. 2013; Foolen et al. 2011). The inner layer is composed of osteoblasts and mesenchymal stem cells, while the outer fibrous layer is composed of collagen, fibroblasts and elastin (Evans et al. 2013). This outer layer provides bone mechanical strength (Allen et al. 2004; Yiannakopoulos et al. 2007).

The knowledge of the mechanical properties of the mandibular periosteum is fundamental to understand its role in osteogenesis distraction and is a preliminary step to define a bone periosteal 3D printing model for testing fractures and osteosynthesis materials. Recently, for the first time, our group has characterized human mandibular periosteum as a viscoelastic material with a typical strongly nonlinear stress–strain curve composed of two phases: low- and high-stiffness phases (Debelmas et al. 2018). The shape and dimensions of the human mandible restrict the amount of retrievable periosteum samples. Several studies already interested to biomechanical properties of periosteum (Zeng et al. 2003; Yiannakopoulos et al. 2007; McBride et al. 2011); for example, Popowics et al. (2002) had studied the biomechanical properties of pig's periosteum from different locations (i.e., mandibular body, zygomatic arch and metacarpal), and Bertram et al. (1998) studied the periosteum from the tibiotarsus of white leghorn chicks for different ages. According to these studies one can conclude that—alike the skin—the periosteal mechanical properties vary

✉ Jeremy Dallard
jeremy.dallard@ensta-paristech.fr

Natacha Kadlub
natacha.kadlub@aphp.fr

Jean Boisson
jean.boisson@ensta-paristech.fr

¹ Unit of Maxillofacial and Plastic Surgery, Necker Enfants Malades, Paris Descartes, Paris, France

² UME, ENSTA Paris, Palaiseau, France

across species and anatomical locations. Therefore, the calvaria bone could provide a large amount of periosteum from the same anatomical area and the same embryologic origin than the mandible. To our knowledge, no comparison study was carried out between these two areas in same species.

According to the literature, human tissues—mainly composed of collagen fibers as the ligament (Weiss et al. 1996)—are generally considered as incompressible. Globally biological soft tissues are considered as incompressible (Dandekar et al. 2003; Sommer et al. 2013). Thus, in this study, the human periosteum will be considered as incompressible. Periosteum collagen fibers are mostly oriented along the bone long axis direction with a wavy appearance (Ellender et al. 1988). Upon stretch, the fibers lines up, like in the skin. As both tissues (skin and periosteum) are composed of collagen and elastin, it is likely their tensile test curves share similar shape. To study skin mechanical properties, Manschot and Brakkee (1986) had proposed a model, based on these microstructural collagen properties. The model neglects the elastin contribution and is based on a structural approach involving the mechanical properties of the corrugation of collagen fibrils.

The aim of this study is to test this model on the mandibular periosteum. In addition, we compared mandibular and calvarial periosteum biomechanical properties.

2 Material and method

2.1 Periosteum sample harvest and histological assessment

The same protocol as in Debelmas et al. (2018) is used in this article. From January to June 2017, nine human cadavers (three males and six females) were dissected (numbered from I to IX) (Ecole de Chirurgie, Agence Générale des Equipements et Produits de Santé-AGEPS, Assistance Publique Hopitaux de Paris-APHP, APHP). Permission to perform cadaveric study on cadaveric specimens was obtained from the institutional review board (Ecole de Chirurgie, AGEPS, APHP). Ages at death ranged from 75 to 97 years. Lengths of preservation in cold (at -18°C) extended from 13 to 460 days (Verstraete et al. 2015). For each subject, one vestibular mandibular, one lingual mandibular and serial calvarial periosteum from various locations were harvested with a template of 40 mm per 10 mm. The mandible samples were harvested just behind the alveolar foramen, at an equal distance from the upper and lower edge of the mandible. The calvarial samples were harvested just behind the coronal suture, parallel to the longitudinal suture (see Fig. 1). Dimensions were set before harvesting the tissue to cope with its natural shrinkage. Then, the periosteum was cut following the drawings,

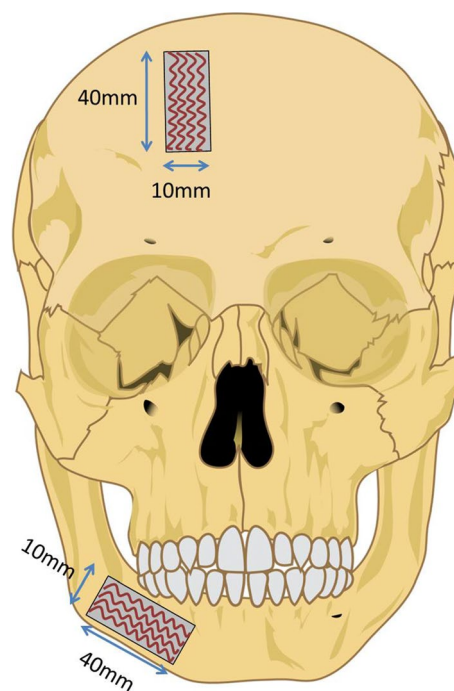


Fig. 1 Scheme of the harvested periosteum locations for the mandible vestibular side and the calvaria. We also reported the collagen fibers orientation according to the literature. The mandible samples are oriented along the mandible long axis in both vestibular and lingual sides

and slices were collected using a sharp elevator and immediately stored in saline solution for transportation to location of the tensile test machine. Specimens were taken out of their saline solution a few hours after being harvested and were suspended 10 min in ambient air in a vertical position, to drain the excess water. The objective of this procedure was to avoid desiccation and to limit the artifact due to tissue swelling.

Separate samples (5 per 10 mm) of each periosteal specimen were harvested at the posterior end of the specimens just before storage in saline solution; then, these samples were immediately fixed in formol and embedded in paraffin. Four μm -thick sections were cut from each paraffin block. Staining with hematoxylin/eosin/saffron (HES) was automated using a Leica Autostainer (Leica Biosystems GmbH, Nussloch, Germany). The sections were mounted in synthetic resin (WVR International, Radnor, PA, USA). The mean thickness (h) of the periosteum was measured on cross-sectional slides (averaged on five random thickness measures for each sample) using ImageJ version 1.48 (public domain software, National Institutes of Health, Bethesda, MD, USA). For each specimen, a photograph of three randomly selected 400 \times magnification fields had been taken by Leica DMI8s microscope platform (Leica MicrosystemsTM, Wetzlar, Germany).

2.2 Parameters and tensile protocol

Tensile tests were performed with an uniaxial elongation machine (3342 Single Column, Instron Corp., Illinois Tool Works Inc., Glenview, IL, USA) at room temperature (18–20 °C). Each periosteal sample was moistened every 3 min during the experiment using an atomizer (Fig. 2a). Periosteum slice ends were secured in two grips connected to the elongation device. The distance between the grips is controlled at a precision of 0.01 mm. The bottom jaw was fixed on the machines base; the upper jaw could move at a specified speed in the vertical direction and was connected to a load cell with a 100 N capacity (2519 series, Instron Corp., Illinois Tool Works Inc.). In terms of orientation, tension is applied along stress fiber axis.

Stress is defined as a load normalized on a surface. Hence, we have:

$$\sigma = \frac{L}{w \times h} \quad (1)$$

where σ is the axial stress in pascals (Pa), L is the load in newtons (N) recorded by the load cell (see above for the load cell characteristics) and $w \times h$ is the initial cross-sectional area of the specimen (in m^2) perpendicular to the stretching direction; h is the thickness of the periosteum measured on histology slice (see above); and w is the initial width of periosteum sample measured on the bone.

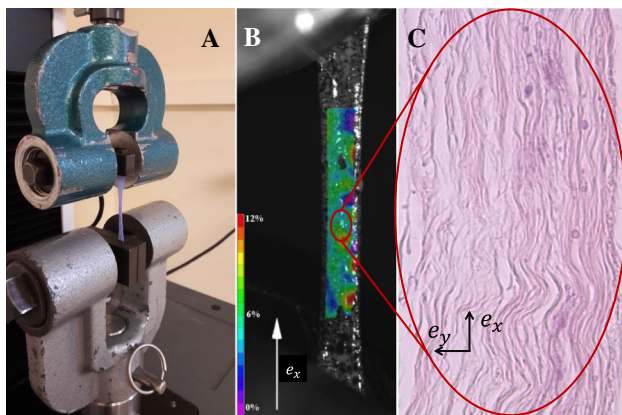


Fig. 2 **a** Picture of the tensile test apparatus. The elongation procedure was recorded with a high resolution video camera. The speckled periosteal sample can be seen between the grips of the machine. **b** Example of axial strain homogeneity on vestibular mandibular periosteum (cadaver IV). Tensile tests were recorded, and Lagrange deformation fields were calculated using digital image correlation. The Vic-2D parameters used to perform this analysis included a step of 3 pixels, Gaussian subset weights, optimized 8-tap interpolation, normalized square differences and incremental correlation. The consistency threshold was set at 0.05 (maximum margin), and the maximum confidence margin was 0.05. In this figure, the axial strain ($\bar{\epsilon}_x$) is displayed with a color scale. **c** Picture at zoom $\times 400$ of a histological slice of a periosteum sample taken from the vestibular part. We assume, from the histological analysis, that the collagen fibril are aligned with the same axis. The sample is oriented in order to align the fibril collagen corrugation with $\bar{\epsilon}_x$

Elongation is defined as:

$$\epsilon_g = \frac{\Delta l}{l} \quad (2)$$

where Δl is the variation of distance between the two jaws measured during the tensile test and l is the initial distance between the jaws.

All specimens underwent the same tensile protocol elaborated using Bluehill 3 software (Instron, Illinois Tool Works Inc.), which consisted of two phases: phase 1: a continuous traction at a rate of 0.25 mm/s until 15% deformation: $\epsilon_g = 0.15$ and phase 2: a 300 s relaxation at $\epsilon_g = 0.15$.

2.3 Elongation homogeneity

In order to demonstrate the homogeneity of the deformation during an uniaxial tensile test, elongation in the central region of the five samples was measured using digital image correlation (DIC). Samples were speckled using India ink, and periosteal elongation was recorded using a 5-megapixel-resolution video camera (GO-5000M-PMCL, JAI, Copenhagen, Denmark). Images were processed using Vic-2D version 6.0.6 digital image correlation software (Correlated Solutions, Inc., Irmo, SC, USA) to compute the Lagrange deformation fields of the samples. The measured strain in the central region is linear with $\frac{\epsilon}{\epsilon_g} = k$. Therefore, we corrected the strain ϵg by this coefficient to determine the strain ϵ of the sample homogeneous region. For the samples where the DIC was not available, we have corrected ϵg by the average coefficient \bar{k} calculated on the other experiments. In the following, we only consider the strain of the homogeneous region $\epsilon (\epsilon = \epsilon_g \cdot \bar{k})$.

2.4 Tensile test model

2.4.1 Phase 1

The objective here was to use a model with mainly geometric parameters that we could also measure using imaging on the histological slices. The periosteum presents a typical nonlinear stress–strain curve with a similar shape as the skin. Ellender et al. (1988) showed that the collagen fibrils of periosteum are aligned with the long axis of the bone. Therefore, we used the model based on a collagen structural approach developed by Manschot and Brakkee (1986) for the skin. This model is considering the collagen fibril like an elastic rod with a planar sinusoidal waveform and neglects any contributions from other components (elastin). It also supposes that the tensile force is applied along the fibrils' direction; then, the straining process is decomposed into two parts.

First part, the collagen fiber is straightened; thus, it is the collagen bending stiffness which is contributing to the

stress–strain curve. This corresponds to the low-stiffness region of the tensile test curve.

Second part, the fiber is straight; thus, the stress is originated from elastic behavior of the collagen (E_c). This corresponds to the high-stiffness region of the tensile test curve. More details can be found in Comninou and Yannas (1976).

The stress–strain curve related to the model is

$$\epsilon = \frac{(\mu + 1)(\frac{\sigma}{E_c} + 1)}{1 + \mu\gamma^2} - 1 \tag{3}$$

with

$$\gamma = \frac{1}{C_F \frac{\sigma}{E_c} (\frac{\sigma}{E_c} + 1) + 1}. \tag{4}$$

The three model parameters E_c , C_F and μ are related to structural material properties of the tissue.

E_c is a material parameter representing the collagen elasticity.

$$E_c = E_{coll}\rho \tag{5}$$

where E_{coll} is the Young’s modulus of pure collagen and ρ is a measure for the surface fraction occupied by the collagen in the periosteum.

C_F represents the typical corrugation of the fibril,

$$C_F = \frac{\lambda_0}{\pi R} \tag{6}$$

with λ the fibril wavelength and R its typical circular section radius.

μ is related to the elongation value at which the fibril has become almost straight.

$$\mu = \frac{\tan^2 \theta}{4} \tag{7}$$

with θ the maximum angle of the sinusoidal shape of the collagen fibril with its main direction (Fig. 2c).

On the tensile test curve, E_c is related to the final stiffness, μ to the elongation where the stiffness change arises (between the low- and high-stiffness regions) and C_F to the low-stiffness region and to the curvature of the transition between the low- and high-stiffness regions. In the following, using the model, we will fit the tensile test curves to extract the parameters from periosteum from different locations to compare their mechanical properties.

2.4.2 Phase 2

For phase 2, the stress over time relation $\sigma(\epsilon, t)$, normalized by the stress at the beginning of the relaxation σ_{coll} , was fitted with the bi-exponential function

$$\text{Phase 2 : } \sigma(\epsilon, t)/\sigma_{coll} = A(e^{-t/\tau_1} + e^{-t/\tau_2}) + \sigma_{\infty}, \tag{8}$$

providing two characteristic times, τ_1 and τ_2 , specific to each periosteal sample Lynch et al. (2017). σ_{∞} is the residual stress over σ_{coll} . These tests are applied in both calvarial and mandibular specimens.

2.5 Slice image treatment

According to the Manschot model, E_c , μ and C_F are related to the material and structure properties of the collagen tissue. The objective is to measure structural properties of the periosteum on histological slices and compare them to the parameters extracted from the model (Fig. 2c). On each histological slice, we took three pictures at a zoom of 40× at different locations with taking care of align the collagen fibers with the \vec{e}_x direction. Then, for the three pictures, we calculated the spatial spectrum on each line along the \vec{e}_x direction, and we averaged these spectra over \vec{e}_y direction. We also did the opposite: calculating the spatial spectrum on each column along the \vec{e}_y direction, and we averaged these spectra over \vec{e}_x direction. These averaged spectra extract predominant characteristic lengths of the periosteum structure in the \vec{e}_x and \vec{e}_y directions.

For each direction, we identified in averaged spectra: two peaks corresponding to two wavelengths (Fig. 3).

Small wavelengths $\lambda_{x,1}, \lambda_{y,1} \sim 0.6 \mu\text{m}$ which correspond to the characteristic thickness of collagen fiber. According to the literature (Altendorf et al. 2012), this value appears to be relevant—if this peak is not displayed on the spectrum, we took the mean value of similar samples.

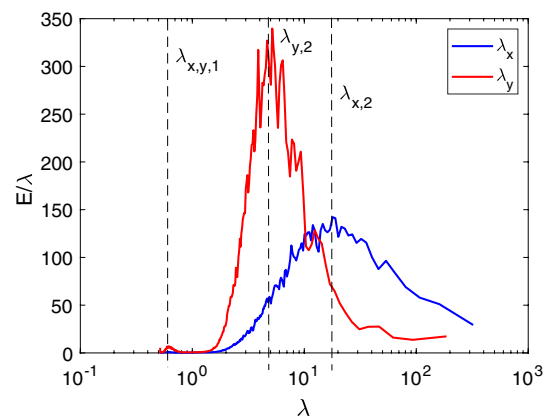


Fig. 3 Example of a spatial spectrum of a histological slice of the vestibular periosteum. Each spatial spectrum presents two peaks pointed by the dashed lines. The peak at small wavelength ($\sim 0.6 \mu\text{m}$) is noted: $\lambda_{x,1}$ and $\lambda_{y,1}$ and the peak at a large wavelength ($\sim 10 \mu\text{m}$) is noted: $\lambda_{x,2}$ and $\lambda_{y,2}$.

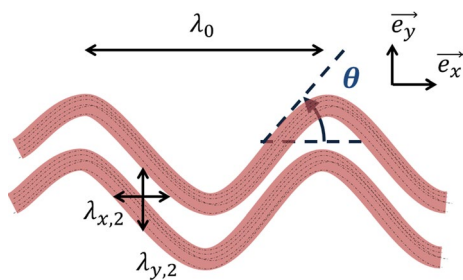


Fig. 4 Collagen fiber scheme and the geometric definition of the typical wavelength extracted from the spatial spectra $\lambda_{x,2}, \lambda_{y,2}$; the corrugation maximum angle (θ) and the corrugation wavelength λ_0

Large wavelengths $\lambda_{x,2}, \lambda_{y,2} \sim 10 \mu\text{m}$ which corresponds to half the characteristic thickness of collagen fibril (Fig. 4).

2.6 Tissue density measure

The collagen density has been measured directly from images of histological slice. The method consisted to enumerate the averaged number of fibers n_F in a reference distance l_y along the y-direction. Therefore, the collagen surface tissue density ρ can be approximated by:

$$\rho \approx n_F \frac{\lambda_{y,2}^2}{l_y^2}, \tag{9}$$

where $\lambda_{y,2}^2$ corresponds to the area of the cross section of a fiber and l_y^2 to the area of the reference cross section of the periosteum. According to the definition of the model parameters: E_c, C_F and μ , these parameters can be related to the structural measures. Here we used a median value for the elastic modulus $E_{\text{coll}} = 1000 \text{ MPa}$ extracted from the literature (Wenger et al. 2007). If we suppose that the collagen fibrils are aligned with the long axis bone (Ellender et al. (1988)), itself aligned with the tensile test stretching direction \vec{e}_x , and that the spatial spectra are dominated by the contribution of the fibril maximum angle corrugation (θ in Fig. 4), then μ can be approximated like:

$$\mu \approx \frac{\lambda_{y,2}}{4\lambda_{x,2}}. \tag{10}$$

Finally, for the three pictures of each histological slice, we measured the fibril's wavelength λ_0 (see Fig. 4). According to the definition of C_F , this parameter can be approximated as:

$$C_F \approx \left(\frac{\lambda_0}{\pi\lambda_{y,1}} \right)^2. \tag{11}$$

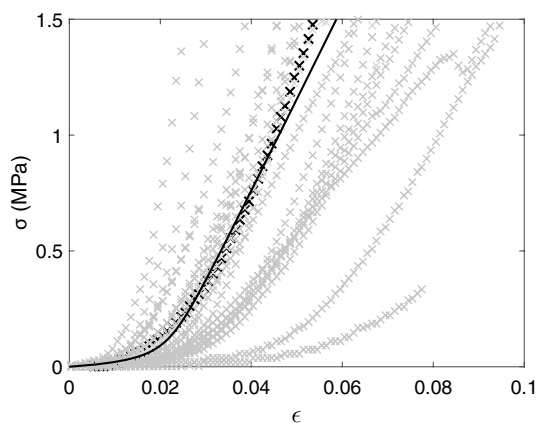


Fig. 5 Phase 1 stress–strain curves of calvaria periosteum. The axial stress σ (in MPa) is displayed against the axial elongation ϵ . We observed typical nonlinear stress–strain curves with a toe region, a heel and a linear steeper phase. Curves of all samples are represented with gray \times . The black curve corresponds to the fit of the traction test of cadaver VII

2.7 Statistical analysis

All the curves were fitted using MATLAB (MathWorks®, Incorporated). Statistical analyses were conducted using IBM®SPSS®Statistics version 23 (IBM®, Chicago, USA). The statistical level of significance was set at $p < 0.05$. Parametric variables normally distributed were displayed with their means and standard deviation (STD) and compared using a t test.

3 Results

3.1 Traction tests and model

3.1.1 Phase 1

The model had been applied to 44 periosteum samples (18 from the mandible: 9 from vestibular and 9 lingual sides; and 26 from calvaria). The typical results of the fitting are shown in Figs. 5 and 6. As expected in collagenic tissues, the curve is composed of two parts: a low- and a high-stiffness region separated by a more or a less smooth transition.

Fitting was accurate in all cases with a typical correlation coefficient $R^2 \sim 0.98$. From the model, the mean resulting parameters are given in Tables 1 and 2.

$$E_{c,\text{mand}} = 18 \pm 17.4 \text{ MPa} \tag{12}$$

$$C_{F,\text{mand}} = 0.98 \pm 1.46 \times 10^3 \tag{13}$$

$$\mu_{\text{mand}} = 0.03 \pm 0.01 \tag{14}$$

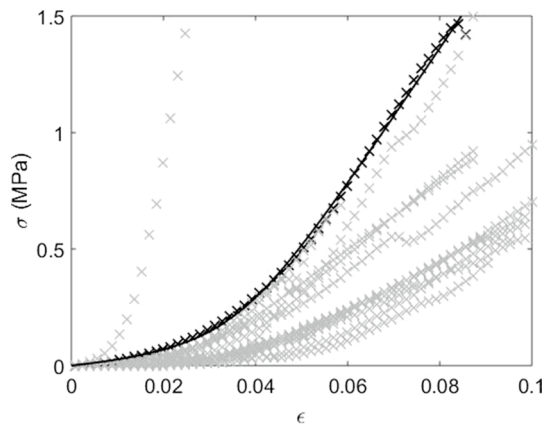


Fig. 6 Phase 1 stress–strain curves of mandibular periosteum. The axial stress σ (in MPa) is displayed against the axial elongation ϵ . We observed typical nonlinear stress–strain curves with a toe region, a heel and a linear steeper phase. Curves of all samples are represented with gray \times . The black curve corresponds to the fit of the traction test of cadaver VII

$$E_{c,calv} = 70.1 \pm 71.4 \text{ MPa} \tag{15}$$

$$C_{F,calv} = 0.82 \pm 0.48 \times 10^3 \tag{16}$$

$$\mu_{calv} = 0.03 \pm 0.01 \tag{17}$$

Table 1 Parameters from model fitting of the tensile test curves and relaxation curve for mandibular periosteum

Cad.	Loc	E_c (MPa)	$C_F \times 10^{-3}$	μ	τ_1	τ_2
I	v	8.4	1.57	0.033	127.8	9.6
	l	10.0	0.78	0.034	122.1	10.1
II	v	7.9	0.45	0.029	122.8	8.4
	l	9.5	0.79	0.032	99.4	8.4
III	v	30.8	0.20	0.035	388.5	68.1
	l	10.8	0.38	0.051	107.9	8.7
IV	v	80.9	0.05	0.010	74.0	6.1
	l	27.6	6.65	0.034	99.3	6.3
V	v	13.2	0.22	0.029	75.4	5.5
	l	9.8	0.41	0.019	107.2	9.3
VI	v	28.0	0.52	0.034	126.5	7.5
	l	21.2	1.36	0.026	134.8	11.6
VII	v	14.1	0.98	0.023	62.8	6.6
	l	16.1	1.25	0.029	92.4	7.7
VIII	v	10.7	1.17	0.043	100.6	5.7
	l	4.3	0.26	0.023	143.8	9.7
IX	v	8.2	0.19	0.019	105.1	8.9
	l	11.7	0.42	0.039	128.7	10.5
Mean (STD)	v	22.5 (23.5)	0.59 (0.52)	0.02 (0.009)	131.5 (99.4)	14.0 (20.3)
	l	13.4 (7.1)	1.30 (2.01)	0.03 (0.009)	115.1 (17.9)	9.1 (1.6)
p vestibular versus lingual		0.29 (NS)	0.29 (NS)	0.44 (NS)	0.63 (NS)	0.48 (NS)

Vestibular and lingual parameters are compared
 NS nonsignificant results, STD standard deviation

The comparison of model parameters between vestibular and lingual mandibular periosteum does not show significant differences (Table 1). However, the stiffness of the collagen (defined in the model by E_c) was significantly higher in calvarial periosteum (Table 2).

3.1.2 Phase 2

From relaxation test, we fitted the curves with the bi-exponential function with R^2 superior to 0.98, giving τ_1 of 123.3 s for the mandible and 96, 5 s for the calvaria, and a mean τ_2 of 11.6 s for the mandible and 7.4 s for the calvaria (Tables 1, 2, and in Figs. 7, 8). Relaxation times were comparable between lingual and vestibular periosteum, and between the mandibular and calvarial periosteum.

3.2 Analysis from collagen structural properties

Structural analysis had been conducted on 10 mandibular specimens (5 vestibular and 5 lingual). From the structural analysis, the mean resulting parameters are reported in Table 3. Statistical analysis showed significant differences between geometric data and traction data for μ , the parameter related to the elongation value for which corrugated

Table 2 Parameters from model fitting of the tensile test curves for calvarial periosteum

Cad.	Value	E_c (MPa)	$C_F \times 10^{-3}$	μ	τ_1	τ_2
I	–	48.0	0.32	0.04	97.4	7.3
II	Mean	60.0	0.80	0.03	123.3	9.4
	STD	40.3	0.27	0.004	97.4	7.3
III	Mean	140.6	0.86	0.03	134.8	10.0
	STD	131.6	0.17	0.01	111.1	8.3
IV	Mean	47.2	0.47	0.03	80.4	6.0
	STD	19.6	0.12	0.01	70.8	6.2
V	Mean	37.0	0.68	0.02	106.8	9.6
	STD	17.3	0.17	0.003	114.5	10.0
VI	Mean	49.8	0.75	0.04	85.6	5.2
	STD	30.0	0.40	0.02	105.5	7.5
VII	Mean	93.7	1.37	0.02	84.3	5.3
	STD	104.1	0.94	0.004	42.8	3.9
Mean calv. (STD)		70.1 (71.4)	0.82 (0.48)	0.03 (0.01)	96.5 (24.1)	7.4 (2.0)
Mean mand. (STD)		18.0 (17.4)	0.98 (1.46)	0.03 (0.01)	123.3 (69.8)	11.6 (14.2)
<i>p</i> calv. versus mand.		0.001 (*)	0.67 (NS)	0.26 (NS)	0.20 (NS)	0.30 (NS)

Calvarial and mandibular parameters are compared
NS nonsignificant results, *STD* standard deviation
 *Highly significant

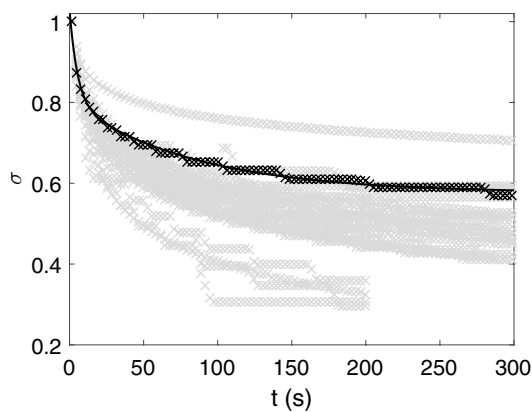


Fig. 7 Calvaria relaxation curves. All samples are represented (gray points); the dark line represents the bi-exponential fit for sample 12. The axial stress σ (in MPa), normalized with the maximum axial stress of the sample max obtained at the end of phase 1, is displayed against time (in s). The following function was used to fit the relaxation curves: $R^2 > 0.983$. It has to be noted that one sample relaxation stopped at 200 s for technical problems. We assume that the relaxation was long enough to perform a bi-exponential fit

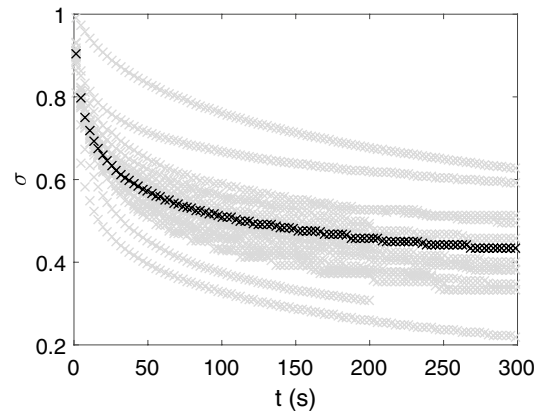


Fig. 8 Mandibular relaxation curves. All samples are represented (gray points); the dark line represents the bi-exponential fit for cadaver IV. The axial stress σ (in MPa), normalized with the maximum axial stress of the sample max obtained at the end of phase 1 is displayed against time (in s). The following function was used to fit the relaxation curves: $R^2 > 0.983$. It has to be noted that one sample relaxation stopped at 200 s for technical problems. We assume that the relaxation was long enough to perform a bi-exponential fit

fibril has become straight. E_c (related to the collagen stiffness) and C_F (corrugation of the fibril) were significantly comparable (Table 3).

Finally, to illustrate those differences we propose a comparison of the Manschot model based on fitted material parameters and parameters identified from histological slices (Fig. 9). We observe a good agreement between the model based on fitted material constants and the results extracted from the tensile tests. The final slope is globally equivalent

between all curves due to low differences between the two values of E_c identified. More specifically, the model based on the histological slices study is the one exhibiting the less stiff behavior. Inflection point location shows a significant difference and is observed around 4% and around 11%, respectively, for the fitted model and for the histology-based model. Influence of μ is also observed thanks to the validity domain of the histology-based model defined by $\mu \pm SD$.

Table 3 Data from collagen histological analysis (mandibular periosteum)

Cad.	E_c (MPa)	$C_F \times 10^{-3}$	μ
	Mean (STD)	Mean (STD)	Mean (STD)
III	20.6 (9.6)	0.42 (0.13)	0.11 (0.10)
IV	8.0 (6.5)	0.31 (0.21)	0.13 (0.06)
V	9.8 (4.9)	0.50 (0.26)	0.05 (0.03)
VI	16.4 (6.3)	0.46 (0.31)	0.13 (0.08)
VII	15.0 (10.8)	0.93 (1.10)	0.08 (0.05)
Mean (histo.)	14.0 (152)	0.53 (0.55)	0.10 (0.07)
Mean (tract.)	18.0 (17.4)	0.98 (1.46)	0.03 (0.07)
p (histo. vs. tract.)	0.30	0.23 (NS)	0.0001 (**)

E_c , C_F , μ were obtained from geometric analysis of the collagen from histological slices. Geometric E_c , C_F , μ were compared to E_c , C_F , μ obtained from the model fitting of the tensile test curves

NS nonsignificant results, STD standard deviation

**Highly significant

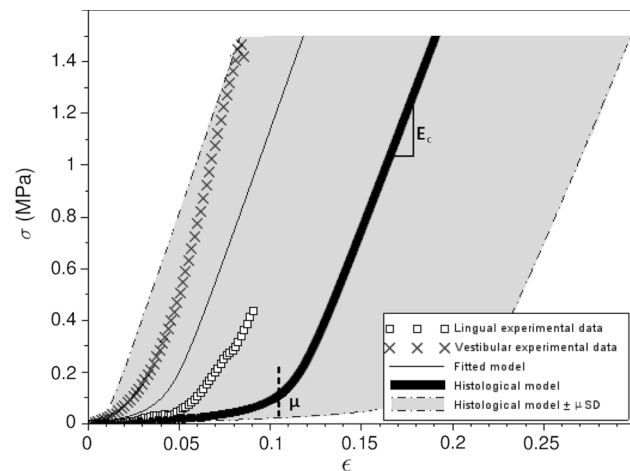


Fig. 9 Comparison of the Manschot model based on material parameters fitted (black line) and parameters identified from histological slices (bold line). In addition, histological models involving extreme values of $\mu \pm SD$ are included inside the light gray area. Corresponding experimental data (Cadaver III) are also proposed represented by cross (vestibular) and white square (lingual)

4 Discussion

4.1 Tensile tests model

In this article, the model proposed by Manschot and Brakkee (1986) for the skin has been tested on the periosteum. To our knowledge, the Manschot and Brakkee (1986) model had only been applied to skin, until now (Wong et al. 2016; Jacquet et al. 2017; Killaars et al. 2015). This model is valid to describe the stress–strain curves, but its link with the periosteum structure is more questionable. In numerous studies,

the stress–strain curve of the periosteum showed a J-shaped pattern, similar to other collagen-rich soft tissues, e.g., the skin (Yiannakopoulos et al. 2008; Eyre-Brook 1984). The periosteum, alike the skin, is composed of a collagenous matrix and few elastin fibers (Dwek 2010). In this context, this was expected that this model could be applied to all collagen-rich tissue, e.g., periosteum, tendon. Finally, the relevance of this model for periosteum is corroborated by the microstructure we observed in pictures of the histological periosteum slice (see Fig. 2c).

In our study, tensile test had been analyzed without preconditioning. Preconditioning is considered as a necessary step to extract the mechanical characteristics of biological tissue (Liu and Yeung 2007). Preconditioning is supposed to align collagen fibers with the stretching direction (Miller et al. 2012), resulting in more consistent data from mechanical testing. In this study, there is no preconditioning for three major reasons: The objective was to compare data from traction test and from histological slice geometric analysis (harvested without conditioning). According to the literature, the periosteum collagen fibers are generally aligned with the long axis of the bone (Ellender et al. 1988). The mechanical stretch was performed along this same direction (Fig. 2c). Finally, the objective was to compare our results with *in vivo* measures like the torque implied in osteogenic distraction.

Analysis of the parameters extracted from the model, in particular E_c , is a first step to evaluate the forces involved in process implying periosteum stretching and remodeling like distraction osteogenesis, fracture and growth. E_c extracted from the stress–strain model fitting is similar to the elastic modulus of the stiff part of the J-shaped curve (from our previous work) [debelmas], respectively, 18 MPa and 18.9 MPa.

Since the periosteum is not exclusively composed of collagen, it is likely that E_c is below the typical modulus of pure collagen (E_{collagen}). According to Wenger et al. (2007), collagen elastic modulus varied from 200 to 11,000 MPa, whereas Manschot and Brakkee (1986) considered a collagen elastic modulus of 100 MPa. In our studies, we used a value of $E_{\text{collagen}} = 1000$ MPa. Hence, the typical value of $E_c \approx 18$ MPa implies that the collagen represents less than 2% of the periosteum volume fraction. This volume fraction is very low and was somewhat unexpected.

The comparison between the parameters extracted from the tensile test fit and the ones extracted from the histological slices analysis is not fully satisfactory. For the μ parameter, the results are significantly different and it has to be noted that the uncertainties for E_c are very important.

The difference in the μ parameter and the large uncertainties for E_c come from many origins:

- The approximation we used to evaluate the histological slice parameters could lead to erroneous results because the periosteal tissue is much more disordered than the

“ideal” image of collagen (Figs. 2c vs. 4) on which we based our reasoning. Evaluating the collagen geometry (e.g., corrugation’s wavelength and amplitude) from the spatial spectra maximum could be a too crude approximation. This could be improved by a statistical approach, evaluating the collagen geometry as the ensemble of the values taken by the spatial spectra and introducing them in the model.

- The difference of conservation condition between histological samples and samples submitted to the tensile test could lead to different shrinkage levels for the same tissue. As the parameter μ is related to the transition elongation between the low- and high-stiffness regions of the tensile test curve, its value is influenced by the shrinkage. Therefore, the statistical difference of μ values between histological and tensile test analysis could be explainable by this shrinkage difference. This discrepancy could be removed with preconditioning the periosteum before both histological fixation and tensile test.
- The collagen elastic modulus we used $E_{\text{coll}} = 1000$ MPa is a typical value extracted from several studies (Strasser et al. 2007; Heim et al. 2006; Grant et al. 2009; Wenger et al. 2007). The uncertainties on this value are very important and are the origin of very large uncertainties on the E_c calculated from histological slices (152 MPa). The collagen elastic modulus values in human periosteum are the main bias of this model and this study and should further be explored.

The comparison between histological slice and tensile test is encouraging, and the development of simultaneous tensile test and imaging would be very interesting to conclude the relation between the tissue structure and its mechanical properties.

4.2 Comparison calvaria/mandible

In order to increase the number of samples, it has been proposed to include periosteum from the same anatomical region (calvarial) and species. In the preamble, we wanted to compare the mechanical properties between the mandible and calvarial periosteum. From stress–strain curve, it has been shown significant differences between the two periosteum, especially regarding E_c . E_c was significantly higher in the calvaria, implying either a higher density of collagen or a stiffer collagen. C_F was comparable between calvaria and mandible, implying a similar wavelength of the collagen fibril. μ was comparable between the two localizations. The tensile test model fit suggests that stiffness is higher in periosteum calvaria related to a stiffer collagen or a higher collagen fraction at this location. As mentioned earlier, several studies had ever showed mechanical differences between periosteum from different bones in a same species. Popowics

et al. (2002), in pigs, showed differences between metacarpal, mandibular and zygomatic periosteum. Additionally, they demonstrated that mandibular periosteum was more deformable than the zygomatic and metacarpal diaphyseal periosteum that is to say with the lowest peak strain and the least strength. These results suggest that harvesting calvaria periosteum to increase the number of samples should be excluded. The large standard deviation observed for calvarial periosteum of the same anatomical subject highlighted the probable variability of periosteum structure into the calvaria.

5 Conclusion

In this study, the mandibular and calvarial periosteum through both tensile test and histological slice analysis have been studied. We demonstrated that the model developed by Manschot and Brakkee (1986) is correct to fit the stress–strain curves for both periosteum tissues. We also showed that its relationship with the observed structure of the periosteum is questionable. This should require a specific study with, for example, a recording of the microstructure during the tensile test and statistical approach to extract a “homogenized” collagen structure. The comparison between calvaria and mandible periosteum shows significant differences that prevent the use of calvarial periosteum to increase the number of samples in a maxillofacial periosteum study, but it also questions the role and origin of a stiffer periosteum in the calvaria than in the mandible. The proposed study provides a behavior law and values of the associated material parameters in order to develop predictive model of the periosteum behavior under distraction osteogenesis mechanical load. As an example, the development of a predictive analytic model of the force developed by the periosteum during DO would be helpful in order to develop new distraction devices. Another important breakthrough for clinicians is the use of 3D printing for practice, to create cutting guides or to develop new modus operandi. However, to create high-fidelity simulation, one requires deep knowledge of the mechanical properties of each tissue constitutive of the reproduced body part. In this context, due its peculiar localization and behavior, periosteum is one of the most important tissues. A possible future work could be the integration of the section monitoring during the uniaxial tensile test. This would give access to the real stress evolution expressed thanks to the deformed section configuration.

Acknowledgements This study was funded by the Prematuration Project IDEX Paris Saclay. The authors declare that they have no conflict of interest. Experimentations were supported by the Strasbourg Research Osteosynthesis Group, Coline Association, AFIF SSR/PAG Association and NARTMF association. Cadaveric experiment was supported by l’Ecole de chirurgie de l’APHP.

References

- Allen MR, Hock JM, Burr DB (2004) Periosteum: biology, regulation, and response to osteoporosis therapies. *Bone* 35(5):1003–1012. <https://doi.org/10.1016/j.bone.2004.07.014>
- Altendorf H, Decenci re E, Jeulin D, Peixoto PDS, Deniset-Besseau A, Angelini E, Mosser G, Schanne-Klein MC (2012) Imaging and 3d morphological analysis of collagen fibrils. *J Microsc* 247(2):161–175
- Bertram JE, Polevoy Y, Cullinane DM (1998) Mechanics of avian fibrous periosteum: tensile and adhesion properties during growth. *Bone* 22(6):669–675
- Comninou M, Yannas IV (1976) Dependence of stress-strain nonlinearity of connective tissues on the geometry of collagen fibers. *J Biomech* 9(7):427–433
- Dandekar K, Raju BI, Srinivasan MA (2003) 3-d finite-element models of human and monkey fingertips to investigate the mechanics of tactile sense. *J Biomechan Eng* 125(5):682–691
- Debelmas A, Picard A, Kadlub N, Boisson J (2018) Contribution of the periosteum to mandibular distraction. *PLoS ONE* 13(6):e0199116. <https://doi.org/10.1371/journal.pone.0199116>
- Dwek JR (2010) The periosteum: What is it, where is it, and what mimics it in its absence? *Skelet Radiol* 39(4):319–23. <https://doi.org/10.1007/s00256-009-0849-9>
- Ellender G, Feik SA, Carach BJ (1988) Periosteal structure and development in a rat caudal vertebra. *J Anat* 158:173–87
- Evans SF, Parent JB, Lasko CE, Zhen X, Knothe UR, Lemaire T, Knothe Tate ML (2013) Periosteum, bone’s “smart” bounding membrane, exhibits direction-dependent permeability. *J Bone Min Res Off J Am Soc Bone Min Res* 28(3):608–17. <https://doi.org/10.1002/jbmr.1777>
- Eyre-Brook AL (1984) The periosteum: its function reassessed. *Clin Orthop Rel Res* 189:300–317
- Foolen J, van Donkelaar CC, Ito K (2011) Intracellular tension in periosteum/perichondrium cells regulates long bone growth. *J Orthop Res Off Publ Orthop Res Soc* 29(1):84–91. <https://doi.org/10.1002/jor.21224>
- Grant CA, Brockwell DJ, Radford SE, Thomson NH (2009) Tuning the elastic modulus of hydrated collagen fibrils. *Biophys J* 97(11):2985–2992. <https://doi.org/10.1016/j.bpj.2009.09.010>
- Heim AJ, Matthews WG, Koob TJ (2006) Determination of the elastic modulus of native collagen fibrils via radial indentation. *Appl Phys Lett* 89(18):181902. <https://doi.org/10.1063/1.2367660>
- Jacquet E, Chambert J, Pauchot J, Sandoz P (2017) Intra- and inter-individual variability in the mechanical properties of the human skin from in vivo measurements on 20 volunteers. *Skin Res Technol* 23(4):491–499. <https://doi.org/10.1111/srt.12361>
- Killaars R, Penha TRL, Heuts EM, van der Hulst R, Piatkowski AA (2015) Biomechanical properties of the skin in patients with breast cancer-related lymphedema compared to healthy individuals. *Lymphat Res Biol* 13(3):215–221. <https://doi.org/10.1089/lrb.2014.0049>
- Liu Z, Yeung K (2007) The preconditioning and stress relaxation of skin tissue. *J Biomed Pharm Eng* 2(1):22–28
- Lynch B, Bancelin S, Bonod-Bidaud C, Gueusquin JB, Ruggiero F, Schanne-Klein MC, Allain JM (2017) A novel microstructural interpretation for the biomechanics of mouse skin derived from multiscale characterization. *Acta Biomater* 50:302–311
- Manschot JF, Brakkee AJ (1986) The measurement and modelling of the mechanical properties of human skin in vivo-II. The model. *J Biomechan* 19(7):517–21
- McBride SH, Evans SF, Knothe Tate ML (2011) Anisotropic mechanical properties of ovine femoral periosteum and the effects of cryopreservation. *J Biomechan* 44(10):1954–1959. <https://doi.org/10.1016/j.jbiomech.2011.04.036>
- Miller KS, Edelman L, Connizzo BK, Soslowky LJ (2012) Effect of preconditioning and stress relaxation on local collagen fiber realignment: inhomogeneous properties of rat supraspinatus tendon. *J Biomechan Eng* 134(3):031007. <https://doi.org/10.1115/1.4006340>
- Popowicz TE, Zhu Z, Herring SW (2002) Mechanical properties of the periosteum in the pig, *Sus scrofa*. *Arch Oral Biol* 47(10):733–41
- Sommer G, Eder M, Kovacs L, Pathak H, Bonitz L, Mueller C, Regitnig P, Holzapfel GA (2013) Multiaxial mechanical properties and constitutive modeling of human adipose tissue: a basis for pre-operative simulations in plastic and reconstructive surgery. *Acta Biomater* 9(11):9036–9048
- Strasser S, Zink A, Janko M, Heckl WM, Thallhammer S (2007) Structural investigations on native collagen type I fibrils using AFM. *Biochem Biophys Res Commun* 354(1):27–32. <https://doi.org/10.1016/j.bbrc.2006.12.114>
- Verstraete MA, Van Der Straeten C, De Lepeleere B, Opsomer GJ, Van Hoof T, Victor J (2015) Impact of drying and thiel embalming on mechanical properties of achilles tendons. *Clin Anat* 28(8):994–1001
- Weiss JA, Maker BN, Govindjee S (1996) Finite element implementation of incompressible, transversely isotropic hyperelasticity. *Comput Methods Appl Mech Eng* 135(1–2):107–128
- Wenger MP, Bozec L, Horton MA, Mesquida P (2007) Mechanical properties of collagen fibrils. *Biophys J* 93(4):1255–1263. <https://doi.org/10.1529/biophysj.106.103192>
- Wong WLE, Joyce TJ, Goh KL (2016) Resolving the viscoelasticity and anisotropy dependence of the mechanical properties of skin from a porcine model. *Biomechan Model Mechanobiol* 15(2):433–446. <https://doi.org/10.1007/s10237-015-0700-2>
- Yiannakopoulos CK, Kanellopoulos AD, Trovas GP, Dontas IA, Lyritis GP (2007) The biomechanical capacity of the periosteum in intact long bones. *Arch Orthop Trauma Surg* 128(1):117–120. <https://doi.org/10.1007/s00402-007-0433-5>
- Yiannakopoulos CK, Kanellopoulos AD, Trovas GP, Dontas IA, Lyritis GP (2008) The biomechanical capacity of the periosteum in intact long bones. *Arch Orthop Trauma Surg* 128(1):117–20. <https://doi.org/10.1007/s00402-007-0433-5>
- Zeng YJ, Xp Sun, Yang J, Wu Wh, Xu Xh, Yp Yan (2003) Mechanical properties of nasal fascia and periosteum. *Clin Biomechan (Bristol Avon)* 18(8):760–764

Publisher’s Note Springer Nature remains neutral with regard to jurisdictional claims in published maps and institutional affiliations.